(This is a sample cover image for this issue. The actual cover is not yet available at this time.)

Journal of Power Sources 229 (2013) 210–215

Contents lists available at SciVerse ScienceDirect

Journal of Power Sources

journal homepage: www.elsevier.com/locate/jpowsour

Kinetic study of the hydrogen oxidation reaction on Pt over the complete overpotential range

María S. Rau, María R. Gennero de Chialvo*, Abel C. Chialvo

Programa de Electroquímica Aplicada e Ingeniería Electroquímica (PRELINE), Facultad de Ingeniería Química, Universidad Nacional del Litoral, Santiago del Estero 2829, 3000 Santa Fe, Argentina

HIGHLIGHTS

- ► Study of the hydrogen oxidation reaction on the complete overpotential range.
- ► Effect of oxyanions in the inhibition of the reaction at high overpotentials.
- ► Inhibition of active sites due to the reversible electroadsorption of OH species.
- ► Correlation of experimental results through a unique set of kinetic parameters.

ARTICLE INFO

Article history:
Received 29 October 2012
Received in revised form
27 November 2012
Accepted 30 November 2012
Available online 10 December 2012

Keywords:
Hydrogen oxidation
Platinum
High overpotentials
Oxyanion adsorption

ABSTRACT

The hydrogen oxidation reaction (*hor*) is studied on a polycrystalline platinum electrode in H_2SO_4 and $HClO_4$ solutions at different rotation rates in the overpotential region comprised between $0.0 < \eta/V \leq 1.1$. The experimental polarization curves recorded at steady state are quite similar for both acids. The results are interpreted in the whole overpotential region on the basis of the Tafel–Heyrovsky–Volmer kinetic mechanism, coupled with a reversible water electroadsorption step. The experimental results are correlated with the equations derived from the resolution of the kinetic mechanism. A unique set of kinetic parameters can appropriately simulate the polarization curves obtained in both electrolyte solutions for all rotation rates, indicating that the proposed mechanism is suitable for the description of the reaction in the whole range of overpotentials. Moreover, the results indicate that the oxyanions do not play a decisive role in the inhibition of the active sites involved in the reaction, adsorbed OH generated from water electroadsorption being most likely responsible for behaviour at high overpotentials.

1. Introduction

The hydrogen oxidation reaction (*hor*) was studied since the beginning of modern electrochemistry and more recently it has received considerable attention in relation to the development of the H_2–O_2 proton exchange membrane fuel cell (PEMFC) [1–3]. Nevertheless, basic kinetic studies of the reaction carried out on a polycrystalline platinum electrode in acid solutions in well-defined mass transfer conditions are scarce, in spite of Pt being the most used electrocatalyst at the anode of PEMFCs. Moreover, there are only a few studies of the reaction on rotating disc electrodes at high overpotentials, a region where the polarization curves show a marked decrease in current density, after reaching the characteristic plateau at each rotation rate [4–6]. There are also several works of this kind on Pt single crystals [7–9]. Nevertheless, a kinetic model that takes into account such decrease and that describes the behaviour of the reaction on Pt in the whole overpotential region has yet to be proposed.

It is known that on Pt the anions $SO_4^{=}/HSO_4^{-}$ are usually considered as specifically adsorbed, meanwhile the behaviour of ClO_4^{-} corresponds to a non-adsorbing anion [10–12]. Therefore, it should be of interest to study the reaction on both electrolyte solutions in order to elucidate the influence of oxyanions adsorption. On the other hand, it is also known that water electroadsorption takes place at high overpotentials and therefore it cannot be neglected in any kinetic mechanism proposed for the description of the behaviour of the hydrogen oxidation on the complete overpotential range. In this sense, results obtained on a polycrystalline ruthenium electrode were successfully interpreted on terms of the mechanism of Volmer–Heyrovsky–Tafel combined with a water electroadsorption step [13].

* Corresponding author. Tel.: +54 342 457 1164x2519; fax: +54 342 4536861.
E-mail address: mchialvo@fiq.unl.edu.ar (M.R. Gennero de Chialvo).

0378-7753/$ – see front matter © 2012 Elsevier B.V. All rights reserved.
http://dx.doi.org/10.1016/j.jpowsour.2012.11.137

As the design of improved catalysts should be performed on the basis of the most complete knowledge of the reaction mechanistic details, the understanding of the basic kinetic principles that govern the behaviour of the adsorbed species (reaction intermediate and inhibitors) and their role in the reaction under study is essential for the optimization and design of the electrocatalyst. These aspects have not received much attention so far, although they play a decisive role in the overall behaviour of the electrode. In this context, the present work proposes first to analyse whether the inhibition process that takes place in the hydrogen oxidation reaction at high potentials shows a different behaviour in H_2SO_4 and $HClO_4$ solutions, respectively. Following this, a kinetic model is developed to completely describe the reaction, including the inhibition process at high overpotentials.

2. Materials and methods

Measurements were carried out in a three-electrode cell specially built for the use of a rotating electrode. The working electrode was a rotating disc of polycrystalline platinum (Radiometer Analytical SAS, Lyon, France) with a geometric area of 0.07 cm^2. The rotation rate was varied in the range $900 \leq \omega/\text{rpm} \leq 4900$ through the use of a speed control unit Radiometer Analytical EDI10K. The counterelectrode was a platinum helical wire of large area. Two different electrolyte solutions were used, 0.5 M H_2SO_4 and 1 M $HClO_4$, prepared with ultra-pure water, obtained from a PureLab purifier (Elga LabWater), which was fed with bidistilled water. The purity of the solution was verified through the absence of electrooxidation processes different from those characteristics of the Pt electrode in the voltammetric profile obtained after the application of an adsorption step at 0.2 V during 5 min in the deoxygenated solution.

Measurements were carried out at 25 °C under hydrogen gas bubbling at 1 atm, with a particular design of the hydrogen saturator ensuring a continuous saturation of the electrolyte with molecular hydrogen. The applied overpotentials were controlled with respect to a reversible hydrogen electrode in the same solution (RHE) and therefore potentials (E) are coincident with overpotentials (η).

For the determination of the experimental current-overpotential dependences $j_{exp}(\eta,\omega)$, the working electrode was mechanically polished with 1200 grit emery paper and 0.3 μm alumina powder, followed by sonication in ultra-pure water for 5 min. Finally, it was subjected to a potential pulse at 2 V during 30 s, while it was rotated at 4900 rpm, in an auxiliary cell. After the electrode was located in the measurement cell, a stabilized voltammetric profile was recorded in the solution deoxygenated by N_2 bubbling in order to verify the appropriate condition of the electrode surface. The voltammetric responses of the Pt electrode are illustrated in Fig. 1 for both solutions, 1 M $HClO_4$ (Fig. 1a) and 0.5 M H_2SO_4 (Fig. 1b). They are coincident with those shown in the literature [14]. Then N_2 was replaced by H_2, and the open circuit potential decreased to 0.0 ± 0.0005 V, achieving the equilibrium potential of the hydrogen electrode. Starting from these conditions, a potential program was applied for the determination of the experimental current-overpotential dependences at a given rotation rate in the range $0.0 \leq \eta/\text{V} \leq 1.1$. It consisted in a potential step at 1.5 V during 10 s to oxidize any impurity that might be present on the electrode surface, followed by a reduction step at 0.00 V for 1 s, followed by immediately pulsing to a given overpotential value, which was maintained for 600 s in order to ensure the achievement of a constant current value. During this period, readings of current were made each 0.1 s. The mean value of the current data measured in the last 10 s was assigned to the step overpotential. These steps were repeated for each η value in order to always start from the same state of the electrode surface.

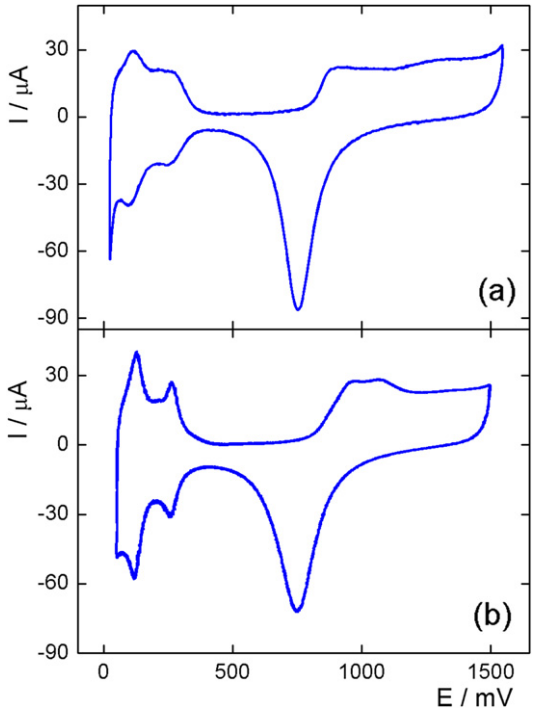

Fig. 1. Potentiodynamic profile of a Pt electrode run under N_2 at 0.1 V s^{-1}; 25 °C. (a) 1 M $HClO_4$; (b) 0.5 M H_2SO_4.

3. Results and discussion

The polarization curves $j(\eta)$ for the hydrogen oxidation reaction were obtained for five different values of rotation rates (900, 1600, 2500, 3600 and 4900 rpm) in both, sulphuric and perchloric acid solutions. They are shown in Fig. 2 (symbols) for the H_2SO_4 solution and in Fig. 3 (symbols) for the $HClO_4$ solution. These results are characterized by the existence of a current plateau in the range $0.05 < \eta/\text{V} \leq 0.6$. Then, the current density decreases, being negligible the values measured for $\eta > 1$ V. It can be observed that the responses in both solutions involve the same range of overpotentials, with small differences in the current values corresponding to the plateau. These are due to differences in the corresponding values of the properties that influence the limiting diffusion current density (molecular hydrogen diffusion coefficient and solubility, solution viscosity). On Pt, it is widely accepted that specific adsorption of SO_4^-/HSO_4^- takes place, while ClO_4^- is usually considered to be a non-adsorbing anion [10–12], it may be concluded that the oxyanion adsorption is not responsible for the inhibition of the *hor* at high overpotentials, in agreement with results obtained by Kita et al. [15]. This behaviour would suggest that only the hydroxyl species produced by water electroadsorption inhibit the active sites. OH_{ad} can be considered a precursor state of the formation of O_{ad}.

In order to perform an interpretation of the experimental dependences, it is necessary to describe the behaviour of the hydrogen oxidation reaction on the Pt rotating disc electrode in the extended overpotentials range $0.0 \leq \eta/\text{V} \leq 1.1$. On the basis of the results obtained, the analysis will be carried through a kinetic mechanism consisting in the elementary steps of Tafel, Heyrovsky and Volmer coupled with the water electroadsorption reaction:

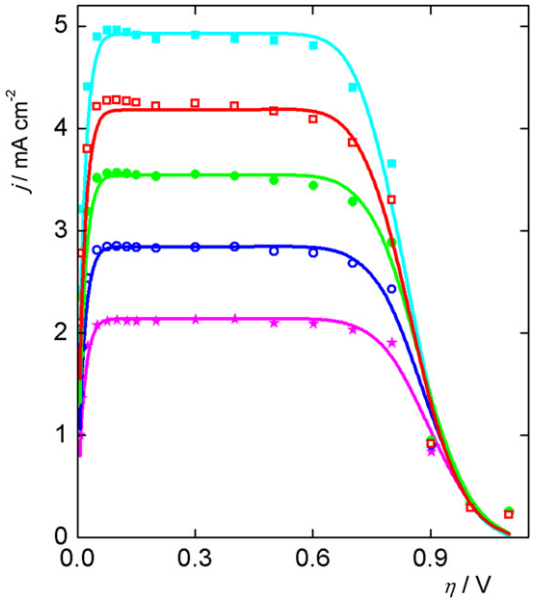

Fig. 2. Experimental (symbols) and simulated (lines) $j(\eta)$ curves of the *hor* on polycrystalline Pt in the range $0.0 \le \eta/V \le 1.1$. 0.5 M H_2SO_4; 25 °C. ω = (★) 900; (○) 1600; (●) 2500; (□) 3600; (■) 4900 rpm.

$$H_2 + 2S \rightleftarrows 2H_{ad} \quad \text{Tafel} \tag{1}$$

$$H_2 + S \rightleftarrows H_{ad} + H^+ + e^- \quad \text{Heyrovsky} \tag{2}$$

$$H_{ad} \rightleftarrows H^+ + e^- + S \quad \text{Volmer} \tag{3}$$

$$S + H_2O \rightleftarrows OH_{ad} + H^+ + e^- \quad H_2O \text{ oxidation} \tag{4}$$

where S represents a site on the electrode surface in which the reaction intermediate H_{ad}, as well as OH_{ad}, can be adsorbed. It should be noticed that the reaction intermediate is weakly adsorbed hydrogen, usually called H_{OPD} (overpotential deposited hydrogen), as accepted from kinetic and spectroscopic evidences [8,16–18]. Consequently, reactions (1)–(3) are the steps of the kinetic mechanism of the hydrogen oxidation, while reaction (4) inhibits surface sites needed for the adsorption of the reaction intermediate. In this sense, it should be noticed that when the *hor* reaches the steady state at a given overpotential, reaction (4) is at the equilibrium state corresponding to this η value. This is because OH_{ad} does not participate directly in the *hor*, but only inhibits hydrogen adsorption sites, and therefore when the potential and the diffusion layer thickness are fixed, the steady state imposes the equilibrium condition for reaction (4). From the resolution of the Tafel–Heyrovsky–Volmer kinetic mechanism at steady state, taking into account the diffusion contribution and considering a Langmuir type adsorption for H_{ad}, the following expressions were obtained [13]:

$$j(\eta, j_L) = \frac{\nu_V^e\left[\frac{\theta_H e^{\beta f\eta}}{\theta_H^e} - \frac{(1-\theta)e^{(\beta-1)f\eta}}{(1-\theta^e)}\right] + \nu_H^e\left[\frac{(1-\theta)e^{\beta f\eta}}{(1-\theta^e)} - \frac{\theta_H e^{(\beta-1)f\eta}}{\theta_H^e}\right]}{\left[\frac{1}{F} + \frac{\nu_H^e(1-\theta)e^{\beta f\eta}}{(1-\theta^e)j_L}\right]} \tag{5}$$

$$j(\eta, j_L) = \frac{\nu_T^e\left[\frac{(1-\theta)^2}{(1-\theta^e)^2} - \frac{\theta_H^2}{\theta_H^{e2}}\right] + \nu_H^e\left[\frac{(1-\theta)e^{\beta f\eta}}{(1-\theta^e)} - \frac{\theta_H e^{(\beta-1)f\eta}}{\theta_H^e}\right]}{\left[\frac{1}{2F} + \frac{\nu_H^e(1-\theta)e^{\beta f\eta}}{(1-\theta^e)j_L} + \frac{\nu_T^e(1-\theta)^2}{(1-\theta^e)^2 j_L}\right]} \tag{6}$$

$$j(\eta, j_L) = \frac{\nu_V^e\left[\frac{\theta_H e^{\beta f\eta}}{\theta_H^e} - \frac{(1-\theta)e^{(\beta-1)f\eta}}{(1-\theta^e)}\right] - \nu_T^e\left[\frac{(1-\theta)^2}{(1-\theta^e)^2} - \frac{\theta_H^2}{\theta_H^{e2}}\right]}{\left[\frac{1}{2F} - \frac{\nu_T^e(1-\theta)^2}{(1-\theta^e)^2 j_L}\right]} \tag{7}$$

where ν_i^e (i = T, H, V) is the equilibrium reaction rate of the elementary step i, β is the symmetry factor of the step i, considered equal for the Heyrovsky and Volmer steps ($\beta_V = \beta_H = \beta$), j_L is the limiting diffusion current density and $f = F/RT$. It should be noticed that in the present case the surface coverage (θ) is the sum of two contributions, the hydrogen coverage (θ_H) and the hydroxyl coverage (θ_{OH}) respectively,

$$\theta = \theta_H + \theta_{OH} \tag{8}$$

Finally, the superscript e indicates the equilibrium condition for the hydrogen oxidation ($\eta = 0$). On the other hand, the dependence $\theta_{OH}(\eta)$ can be obtained from the application of the equilibrium condition to reaction (4), that is accomplished for a given value of η at which the hydrogen oxidation is on steady state. Although it is known that the adsorption of OH_{ad} is appropriately described by a Frumkin or Temkin isotherm [19], for the sake of simplicity and taking into account that in this case OH_{ad} plays a secondary role as inhibitor of active sites, a Langmuir-type adsorption is used. Under these conditions, the following expression is obtained,

$$\theta_{OH} = \frac{\theta_{OH}^e(1-\theta_H)e^{f\eta}}{1-\theta^e+\theta_{OH}^e e^{f\eta}} \tag{9}$$

being θ_{OH}^e the surface coverage of OH_{ad} at $\eta = 0$. It should be noticed that $\theta_{OH}^e \neq \theta_{OH}(\eta)$, although the electrosorption process is at equilibrium. Operating with two of the expressions of $j(\eta, j_L)$, e.g. equations (5) and (6), together with equation (9), an implicit expression for the dependence $\theta_H(\eta, j_L)$ is obtained,

$$\begin{aligned}
&\left\{\nu_V^e\left[\frac{\theta_H e^{\beta f\eta}}{\theta_H^e} - \frac{(1-\theta_H)e^{(\beta-1)f\eta}}{1-\theta^e+\theta_{OH}^e e^{f\eta}}\right] + \nu_H^e\left[\frac{(1-\theta_H)e^{\beta f\eta}}{1-\theta^e+\theta_{OH}^e e^{f\eta}} - \frac{\theta_H e^{(\beta-1)f\eta}}{\theta_H^e}\right]\right\}\times \\
&\left[\frac{1}{2F} + \frac{\nu_H^e(1-\theta_H)e^{\beta f\eta}}{(1-\theta^e+\theta_{OH}^e e^{f\eta})j_L} + \frac{\nu_T^e(1-\theta_H)^2}{(1-\theta^e+\theta_{OH}^e e^{f\eta})^2 j_L}\right] - \left[\frac{1}{F} + \frac{\nu_H^e(1-\theta_H)e^{\beta f\eta}}{(1-\theta^e+\theta_{OH}^e e^{f\eta})j_L}\right]\times \\
&\left\{\nu_T^e\left[\frac{(1-\theta_H)^2}{(1-\theta^e+\theta_{OH}^e e^{f\eta})^2} - \frac{\theta_H^2}{\theta_H^{e2}}\right] + \nu_H^e\left[\frac{(1-\theta_H)e^{\beta f\eta}}{1-\theta^e+\theta_{OH}^e e^{f\eta}} - \frac{\theta_H e^{(\beta-1)f\eta}}{\theta_H^e}\right]\right\} = 0
\end{aligned} \tag{10}$$

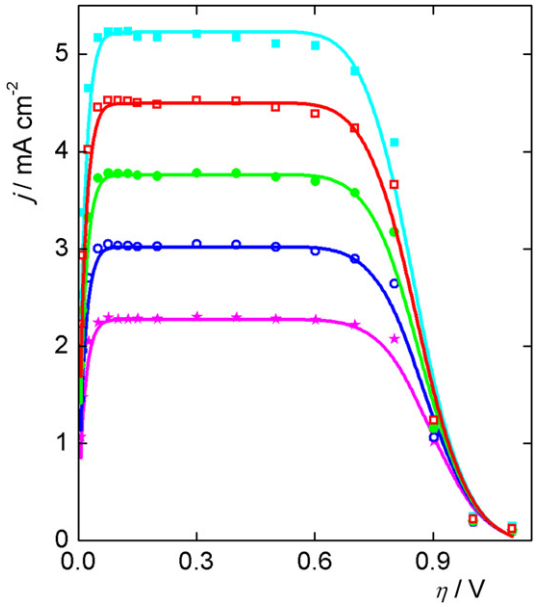

Fig. 3. Experimental (symbols) and simulated (lines) $j(\eta)$ curves of the *hor* on polycrystalline Pt in the range $0.0 \leq \eta/V \leq 1.1$. 1 M $HClO_4$; 25 °C. ω = (★) 900; (○) 1600; (●) 2500; (□) 3600; (■) 4900 rpm.

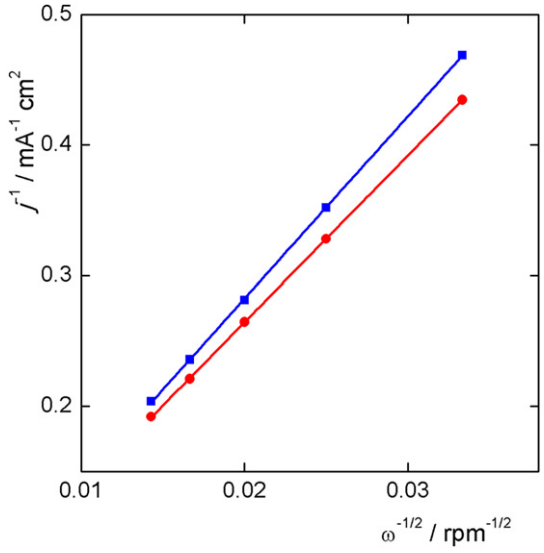

Fig. 4. Dependence of $j^{-1}(\eta = 0.2\ V)$ on $\omega^{-1/2}$. (■) 0.5 M H_2SO_4; (●) 1 M $HClO_4$.

By the use of one of the eqs. (5)–(7), together with equations (8)–(10), the experimental dependence $j(\eta, j_L)$ on steady state corresponding to a given rotation rate can be correlated and the corresponding set of kinetic parameters can be evaluated. It is necessary to evaluate previously the values of j_L for both electrolyte solutions. Taking into account that at low overpotentials ($\eta < 0.40$ V) the dependence $j(\eta, j_L)$ does not depend on step (4), the evaluation of j_L can be carried out from the following relationship, valid in the overpotential range where $\theta = \theta_H + \theta_{OH} = 0$ [20,21]:

$$\frac{1}{j_{max}(\omega)} = \frac{1}{j_{kin}^{max}} + \frac{1}{B\omega^{1/2}} \quad (11)$$

where j_{max} is the current density of the plateau in the $j(\eta, j_L)$ plot, j_{kin}^{max} is the maximum kinetic current density of the Tafel step [19], being $j_{kin}^{max} = 2Fv_T^e/(1-\theta^e)^2$ [19,20] and B is the Levich constant, being $j_L = B\omega^{1/2}$ [22]. It is important to note that the kinetics of the hydrogen oxidation reaction allow the hydrogen surface coverage θ_H to vanish before the surface concentration of molecular hydrogen goes to zero and the current density takes the limiting diffusion value [23]. Under these conditions, and with Tafel–Volmer as the prevailing route at low overpotentials, the current density of the plateau is given by equation (11), the corresponding origin ordinate of the j_{max}^{-1} vs. $\omega^{-1/2}$ plot, which is small but not null. As the potential increases, the Heyrovsky step begins to prevail and finally the diffusion limiting current density is reached. Moreover, the constant B can be obtained from the slope of the straight line. Fig. 4 illustrates such plots for both electrolyte solutions with the experimental current densities corresponding to $\eta = 0.2$ V. The values calculated for B are 7.2 10^{-5} A cm^{-2} $rpm^{-1/2}$ for H_2SO_4 solution and 7.65 10^{-5} A cm^{-2} $rpm^{-1/2}$ for $HClO_4$ solution. Then, considering the symmetry factor equal to 0.5, the experimental $j(\eta)$ curves were correlated applying a non-linear least-square regression method, applying the software Micromath Scientific 3.0, through which the kinetic parameters v_T^e, v_H^e, v_V^e, $\theta_H^e$and θ_{OH}^e were evaluated. Each polarization curve of a given rotation rate was correlated independently. The resulting values of the kinetic parameters corresponding to the 0.5 M H_2SO_4 solution are shown in Table 1, while those corresponding to the 1 M $HClO_4$ solution are given in Table 2. The mean values of the parameters were also calculated, as well as the corresponding standard deviations, which are displayed in the last column of both tables. It can be observed that the mean values of the kinetic parameters in both electrolyte solutions are quite similar. Therefore, a final set of kinetic parameters for the *hor* was calculated from the average of these values, being them: $v_T^e = 7.50 \pm 0.98 \cdot 10^{-7}$ mol cm^{-2} s^{-1}, $v_H^e = 1.40 \pm 0.28 \cdot 10^{-12}$ mol cm^{-2} s^{-1}, $v_V^e = 1.97 \pm 0.04 \cdot 10^{-5}$ mol cm^{-2} s^{-1}, $\theta_H^e = 0.179 \pm 0.03$ and $\theta_{OH}^e = 3.45 \pm 0.79 \cdot 10^{-12}$.

It can be observed that there are differences of several orders of magnitude between the equilibrium reaction rates of the elementary steps. The low value of v_H^e indicates that at low overpotentials the *hor* is mainly verified through the Tafel-Volmer route. Then, as η increases, the reaction rate of the Heyrovsky step increases exponentially while that of the Tafel step decreases. In this sense, it has been found in a previous study [23] that these reaction rates cross each other at $\eta \cong 0.18$ V. Therefore, it can be considered that from this value the Heyrovsky–Volmer route becomes predominant.

Furthermore, the value of θ_{OH}^e indicates that at the equilibrium condition of the hydrogen electrode reaction the adsorption of OH is negligible, which is in agreement which the usual consideration of null coverage in approximated kinetic analysis. In the present case, such an approximation would cancel the dependence $\theta_{OH}(\eta)$ and the inhibition would not take place (equation (9)).

The simulations of the dependencies $j(\eta, j_L)$ for each electrolyte solution are shown as continuous lines in Figs. 2 and 3 respectively. It should be emphasized that they were carried out with only one set of kinetic parameters, corresponding to the mean value of all the correlations made at the different rotation rates in both electrolyte solutions. Even so, the deviations between simulated and experimental values can be considered quite acceptable and similar to those usually found in many regressions illustrated in the literature.

The dependences of the surface coverage of both adsorbed species, H_{ad} and OH_{ad}, on overpotential were also simulated through the use of eqs. (9) and (10) with the calculated kinetic parameters. They are illustrated in Fig. 5(a) and (b) respectively, where it can be appreciated the fast decrease of θ_H, while θ_{OH} becomes to increase from the very low equilibrium value θ_{OH}^e only when $\eta > 0.6$ V, in agreement with the inhibition of the hydrogen

Table 1
Kinetic parameters of the hydrogen oxidation reaction in 0.5 M H_2SO_4.

Kinetic parameters	Rotation rate/rpm					Mean value
	900	1600	2500	3600	4900	
ν_T^e /mol cm^{-2} s^{-1}	$7.60\cdot10^{-7}$	$7.70\cdot10^{-7}$	$7.70\cdot10^{-7}$	$9.00\cdot10^{-7}$	$5.00\cdot10^{-7}$	$7.40 \pm 1.5\cdot10^{-7}$
ν_H^e /mol cm^{-2} s^{-1}	$1.33\cdot10^{-12}$	$1.24\cdot10^{-12}$	$1.22\cdot10^{-12}$	$1.24\cdot10^{-12}$	$1.00\cdot10^{-12}$	$1.21 \pm 0.13\cdot10^{-12}$
ν_V^e /mol cm^{-2} s^{-1}	$1.95\cdot10^{-5}$	$1.90\cdot10^{-5}$	$2.00\cdot10^{-5}$	$2.00\cdot10^{-5}$	$2.00\cdot10^{-5}$	$1.97 \pm 0.05\cdot10^{-5}$
θ_H^e	0.179	0.175	0.175	0.180	0.183	0.178 ± 0.03
θ_{OH}^e	$3.80\cdot10^{-12}$	$3.60\cdot10^{-12}$	$3.60\cdot10^{-12}$	$3.80\cdot10^{-12}$	$1.20\cdot10^{-12}$	$3.20 \pm 1.12\cdot10^{-12}$

Table 2
Kinetic parameters of the hydrogen oxidation reaction in 1 M $HClO_4$.

Kinetic parameters	Rotation rate/rpm					Mean value
	900	1600	2500	3600	4900	
ν_T^e /mol cm^{-2} s^{-1}	$7.70\cdot10^{-7}$	$7.56\cdot10^{-7}$	$7.60\cdot10^{-7}$	$7.60\cdot10^{-7}$	$7.60\cdot10^{-7}$	$7.61 \pm 0.05\cdot10^{-7}$
ν_H^e /mol cm^{-2} s^{-1}	$2.00\cdot10^{-12}$	$1.43\cdot10^{-12}$	$1.49\cdot10^{-12}$	$1.74\cdot10^{-12}$	$1.35\cdot10^{-12}$	$1.60 \pm 0.27\cdot10^{-12}$
ν_V^e /mol cm^{-2} s^{-1}	$2.00\cdot10^{-5}$	$1.90\cdot10^{-5}$	$2.00\cdot10^{-5}$	$2.00\cdot10^{-5}$	$2.00\cdot10^{-5}$	$1.98 \pm 0.05\cdot10^{-5}$
θ_H^e	0.183	0.179	0.183	0.183	0.175	0.181 ± 0.03
θ_{OH}^e	$3.80\cdot10^{-12}$	$3.70\cdot10^{-12}$	$3.60\cdot10^{-12}$	$3.79\cdot10^{-12}$	$3.60\ 10^{-12}$	$3.70 \pm 0.10\cdot10^{-12}$

oxidation reaction. It should be also mentioned that both dependences are almost not influenced by the rotation rates.

Another variable that can be also evaluated from the proposed kinetic model is the relationship between the concentration of molecular hydrogen on the reaction plane and in the bulk respectively ($C_{H_2}^s(\eta)/C_{H_2}^o$), which can be calculated for a given rotation rate with the expression $C_{H_2}^s(\eta)/C_{H_2}^o = 1 - [j(\eta)/j_L]$ [24]. The simulated curves are illustrated in Fig. 5c, where it can be observed that the surface concentration of H_2 decreases at low overpotentials, remains approximately constant between 0.1 and 0.7 V and then increases again, reaching bulk value at $\eta > 1.1$ V. It can be also observed that the relationship $C_{H_2}^s(\eta)/C_{H_2}^o$ is influenced by the rotation rate.

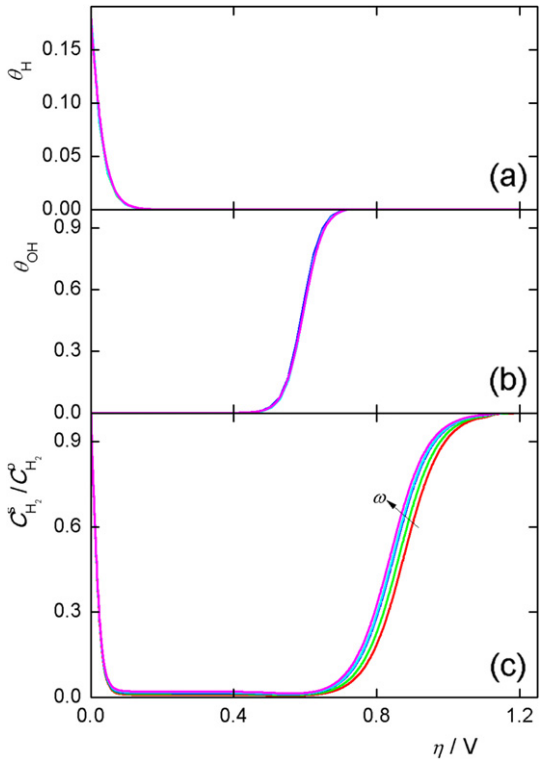

Fig. 5. Dependence of the surface coverage of adsorbed hydrogen (a) and hydroxyl (b) and the surface concentration of molecular hydrogen (c) on overpotential for the *hor* at different rotation rates.

On the other hand, taken into account that a unique set of kinetic parameters can appropriately describe the behaviour of the hydrogen oxidation reaction on polycrystalline Pt electrodes in both electrolyte solutions, it can be concluded that the adsorption of these oxyanions does not play a decisive role in the inhibition of the active sites where the reaction intermediate (H_{OPD}) is adsorbed. This can be explained on the basis of experimental evidences related to the behaviour of sulphate adsorption on the different platinum surfaces. In this sense, there is agreement that (bi) sulphate, and much less perchlorate, are adsorbed at high potentials [25]. However, it should be noted that this conclusion is based mainly on the behaviour of Pt(111), where a maximum $SO_4^{=}/HSO_4^-$ surface coverage of approximately 0.2 was measured [25,26]. The situation changes drastically when the other single crystalline surfaces are analysed. For example, the maximum value of the (bi) sulphate surface coverage on Pt(100) is approximately 0.08 and it takes place at potentials significantly more cathodic than those on Pt(111) [26]. From the analysis of the behaviour of $SO_4^{=}/HSO_4^-$ anions it can be concluded that an appropriate ordering of the Pt surface atoms is needed, which is the case of the threefold configuration of the sulphate adsorption on Pt(111) [27]. On the other hand, the (bi) sulphate adsorption on polycrystalline Pt can be described as the combination of the adsorption on micro and macro facets of the different (*hkl*) with a high degree of defects, which lead to a distinct behaviour with respect to those corresponding to the single crystalline surfaces. For example, the maximum value of the (bi) sulphate surface coverage on Pt(100) is verified at 0.35 V, on Pt(111) at 0.75 V and on polycrystalline Pt at 0.65 V (all vs. RHE) [26]. Recent results obtained on high density of Pt nanoparticles supported using in situ FTIR [28], for which the voltammetric profile corresponds to that of polycrystalline Pt (see Fig. 1 on [28]), showed that oxygenated species (PtOH, PtO, etc.) desorb $SO_4^{=}/HSO_4^-$ anions at 0.75 V (vs. RHE). Moreover, the presence of surface defects (steps, kinks, etc.) characteristic of polycrystalline electrodes prevents the adsorption of (bi)sulphate due to the absence of local surface order, while favours the OH adsorption [29]. Furthermore, taking into account that the surface coverage of $SO_4^{=}/HSO_4^-$ anions decreases as η increases while the inhibition of the *hor* also increases [25], it can be concluded that these oxyanions do not cause the inhibition of the reaction at high overpotentials.

4. Conclusions

The study of the hydrogen oxidation reaction (*hor*) was carried out on a polycrystalline platinum electrode in H_2SO_4 and $HClO_4$ solutions. The polarization curves on steady state were determined in the overpotentials range $0.0 \leq \eta/V \leq 1.1$ at different rotation rates in the range $900 \leq \omega/rpm \leq 4900$. For the analysis of the experimental $j(\eta,\omega)$ dependences, a kinetic model based on the combination of the three steps of the Tafel–Heyrovsky–Volmer mechanism with a reversible water electroadsorption step was used. The parameters involved in the kinetic model were evaluated through the correlation of the experimental results through the use of non-linear least-square regression. Similar values were obtained for all the correlations in both electrolyte solutions. This result indicates that the specific adsorption of $SO_4^{=}/HSO_4^{-}$ should not contribute to the inhibition of the *hor* at high overpotentials, which should be due to water electroadsorption. The influence of the electrolyte was only observed in the different value of the diffusion parameter (Levich constant), while the kinetic behaviour was indistinguishable. The set of kinetic parameters corresponding to the mean value of those obtained in the correlations was used for the simulation of all curves in both electrolyte solutions and for all the rotation rates. The corresponding deviations between the experimental and simulated curves allowed concluding that the proposed mechanism is suitable for the description of the reaction in the whole range of overpotentials.

Acknowledgements

The authors wish to acknowledge the financial support received from ANPCyT, CONICET and UNL.

References

[1] S. Srinivasan, Fuel Cells: From Fundamentals to Applications, Springer, New York, 2006.
[2] F. Alcaide, G. Alvarez, P.L. Cabot, O. Miguel, A. Querejeta, Int. J. Hydrog. Energy 35 (2010) 11634–11641.
[3] J.H. Jang, E. Lee, Yu Kwon, Int. J. Hydrog. Energy 37 (2012) 8170–8176.
[4] V.V. Sobol, A.A. Dmitrieva, A.N. Frumkin, Sov. Electrochem. 3 (1967) 928–932.
[5] V.S. Bagotzky, N.V. Osetrova, J. Electroanal. Chem. 43 (1973) 233–249.
[6] Y.M. Maksimov, O.A. Petrii, A.N. Frumkin, Sov. Electrochem. 10 (1974) 296–300.
[7] N.M. Markovic, B.N. Grgur, P.N. Ross, J. Phys. Chem. B 101 (1997) 5405–5413.
[8] T.J. Schmidt, B.N. Grgur, R.J. Behm, N.M. Markovic, P.N. Ross Jr., Phys. Chem. Chem. Phys. 2 (2000) 4379–4386.
[9] V. Stamenkovic, N.M. Markovic, P.N. Ross Jr., J. Electroanal. Chem. 500 (2001) 44–51.
[10] Y.C. Chiu, M.A. Genshaw, J. Phys. Chem. 73 (1969) 3571–3577.
[11] V. Climent, R. Gomez, J.M. Orts, J.M. Feliu, J. Phys. Chem. B 110 (2006) 11344–11351.
[12] M. Teliska, V.S. Murthi, S. Mukerjee, D.E. Ramaker, J. Phys. Chem. C 111 (2007) 9267–9274.
[13] M.S. Rau, M.R. Gennero de Chialvo, A.C. Chialvo, Electrochim. Acta 55 (2010) 5014–5018.
[14] D.V. Savinova, E.B. Molodkina, A.I. Danilov, Y.M. Polukarov, Russ. J. Electrochem 40 (2004) 683–686.
[15] H. Kita, Y. Gao, T. Nakato, H. Hattori, J. Electroanal. Chem. 373 (1994) 177–183.
[16] J.X. Wang, T.E. Springer, P. Liu, M. Shao, R.R. Adzic, J. Phys. Chem. C 111 (2007) 12425–12433.
[17] Y. Liu, W.E. Mustain, Int. J. Hydrog. Energy 37 (2012) 8929–8938.
[18] K. Kanimatsu, U. Uchida, M. Osawa, M. Watanabe, J. Electroanal. Chem. 587 (2006) 299–307.
[19] A. Damjanovic, V. Brusic, Electrochim. Acta 12 (1967) 615–628.
[20] M.R. Gennero de Chialvo, A.C. Chialvo, Phys. Chem. Chem. Phys. 6 (2004) 4009–4017.
[21] P.M. Quaino, M.R. Gennero de Chialvo, A.C. Chialvo, Electrochim. Acta 52 (2007) 7396–7403.
[22] V.G. Levich, Physicochemical Hydrodynamics, Prentice-Hall, Englewood Cliffs, NJ, 1962.
[23] P.M. Quaino, J.L. Fernandez, M.R. Gennero de Chialvo, A.C. Chialvo, J. Mol. Catal. A: Chem. 252 (2006) 156–162.
[24] A.J. Bard, L.R. Faulkner, Electrochemical Methods: Fundamental and Applications, second ed., John Wiley & Sons, New York, 2001.
[25] M. Futamata, L. Luo, C. Nishihara, Surf. Sci. 590 (2005) 196–211.
[26] M.E. Gamboa-Aldeco, E. Herrero, P.S. Zelenay, A. Wieckowski, J. Electroanal. Chem. 348 (1993) 451–457.
[27] J.A. Santana, C.R. Cabrera, Y. Ishikawa, Phys. Chem. Chem. Phys. 12 (2010) 9526–9534.
[28] D. Zeng, Y. Jiang, Z. Zhou, Z. Su, S. Sun, Electrochim. Acta 55 (2010) 2065–2072.
[29] M. Arenz, K.J. Mayrhofer, V. Stamenkovic, B.B. Blizanac, T. Tamayuki, P.N. Ross, N.M. Markovic, J. Am. Chem. Soc. 127 (2005) 6819–6829.